Nanoscale

The Role of Gold Oxidation State in the Synthesis of Au-CsPbX3 Heterostructure or Lead-free Cs2AuIAuIIIX6 Perovskite Nanoparticles

Journal:	*Nanoscale*
Manuscript ID	NR-ART-08-2019-007222
Article Type:	Paper
Date Submitted by the Author:	21-Aug-2019
Complete List of Authors:	Rodriguez Ortiz, Freddy; Texas A&M University System, Chemistry Roman, Benjamin; Texas A&M University System, Chemistry Wen, Je-Ruei; Texas A&M University System, Chemistry Mireles Villegas, Noel; Texas A&M University System, Chemistry Dacres, David; Texas A&M University System, Chemistry Sheldon, Matthew; Texas A&M University, Chemistry

Journal Name

ARTICLE

The Role of Gold Oxidation State in the Synthesis of Au-$CsPbX_3$ Heterostructure or Lead-free $Cs_2Au^IAu^{III}X_6$ Perovskite Nanoparticles

Received 00th January 20xx,
Accepted 00th January 20xx

DOI: 10.1039/x0xx00000x

www.rsc.org/

Freddy A. Rodríguez Ortiz,[a] Benjamin J. Roman,[a] Je-Ruei Wen,[a] Noel Mireles Villegas,[a] David F. Dacres,[a] Matthew T. Sheldon*[a,b]

Here, we report that the oxidation state of gold plays a dominant role in determining the reaction products when gold halide salts are mixed with all-inorganic lead halide perovskite nanocrystals. When $CsPbX_3$ nanocrystals react with Au(I) halide salts, Au nanoparticles are deposited on the surface of the perovskites through the reduction of Au^{1+} ions by the surfactant ligand shell, to produce Au-$CsPbX_3$ heterostructures. These heterostructures preserve comparably high photoluminescence quantum yield (PLQY) and show identical XRD diffractograms as the parent $CsPbX_3$ nanocrystals. In contrast, the reaction of $CsPbX_3$ nanocrystals with Au(III) halide salts promotes complete cation exchange of Pb ions by Au ions in the nanocrystal perovskite lattice. The cation exchange products, $Cs_2Au^IAu^{III}Br_6$ or $Cs_2Au^IAu^{III}Cl_6$, show XRD patterns corresponding to a tetragonal mixed halide perovskite crystal structure and show no visible photoluminescence. This crucial dependence on the oxidation state of the Au ion informs synthetic strategies for producing and optimizing metal-perovskite heterostructures and lead-free perovskite nanoparticles.

Introduction

Hybrid nanoparticles (HNPs) have been extensively studied over the last several years for photocatalytic[1-3] and optoelectronic[4-6] applications owing to the tailored properties that can be achieved by forming disparate nanoscale material interfaces such as metal-semiconductor[7, 8] and semiconductor-semiconductor.[9] In the case of metal-semiconductor HNPs, there has been significant interest in the selective growth of plasmonic metals on semiconductors, especially for photocatalysis, where the metal broadens the absorbance of the semiconductor, and electron-hole pairs generated in the semiconductor can be spatially separated across the metal-semiconductor interface to perform redox chemistry.[10, 11]

Over the past several years, a number of solution-phase synthetic approaches have been used to fabricate metal-semiconductor HNPs, including photochemical and thermal methods, as well as chemical reduction followed by site selective metal deposition.[7, 8, 12] Many of these synthetic routes have been develop for the canonical material system of cadmium chalcogenide nanocrystals, CdX (X = S, Se, Te), [13-16] in which selective facet growth of Au metal has been successfully achieved for a diverse number of shape geometries including colloidal CdX nanorods, tetrapods, and nanowires.[15, 17-20] Such Au-Cd chalcogenide architectures are generally studied for applications in photocatalysis[21] due to their ability to separate charges across the metal-semiconductor interface. This same property leads to the photoluminescence of the semiconductor being entirely quenched,[22] preventing their use in optical applications where emission is a desirable trait, such as in luminescence up-conversion.[23]

Another semiconductor system that has attracted substantial attention in the last several years has been all-inorganic lead halide perovskites (LHPs) with the composition $CsPbX_3$ (X= Cl, Br or I). These all-inorganic LHPs exhibit excellent optical and electronic properties such as high absorption cross sections, extraordinarily long diffusion lengths, and high fluorescence quantum yields (QYs) and have found applications in photonic and optoelectronic technologies such as solution-processed photovoltaic devices, light-emitting diodes (LEDs), and lasers.[24-27] Recently, Balakrishnan and Kamat demonstrated that nanoscale metallic gold can be deposited onto the surface of $CsPbBr_3$ nanocrystals *via* the reduction of Au(III) salts by the nanocrystal surfactant ligand shell, producing Au-$CsPbBr_3$ heterostructures.[28] Interestingly, these Au-$CsPbBr_3$ heterostructures can maintain high band edge emission quantum yields of 70%, in contrast with similar Au-Cd chalcogenide

[a] Department of Chemistry, Texas A&M University, College Station, Texas 77843, United States
[b] Department of Material Science and Engineering, Texas A&M University, College Station, Texas 77843, United States
Email: sheldonm@tamu.edu
†Electronic Supplementary Information (ESI) available: See
DOI: 10.1039/x0xx00000x

heterostructures for which band-edge luminescence is quenched by the presence of Au metal.[29]

However, despite the unique photophysical properties of the Au-$CsPbX_3$ heterostructure geometry, refined synthetic strategies for metal deposition onto the perovskite surface remain a great challenge. The initial report published by Balakrishnan and Kamat revealed that the size of Au nanoparticle deposition and colloidal stability of the perovskite nanocrystals were limited by the concentration of $AuBr_3$ solution added to $CsPbBr_3$ nanocrystals solution. Indeed, a study by our group revealed that good control over the size and location of deposited metal nanoparticles was limited by undesirable side reactions between $AuBr_3$ and $CsPbBr_3$ nanocrystals.[29] When $AuBr_3$ is added to a solution of $CsPbBr_3$ nanocrystals, Au ions can exchange with Pb ions in the nanocrystal lattice. In fact, the addition of high concentrations of $AuBr_3$ to the perovskite solution can result in the complete cation exchange of Pb ions, producing cesium gold(I) gold(III) bromide nanocrystals ($Cs_2Au^{I}Au^{III}Br_6$). In this cation exchange reaction, some of the Au^{3+} ions are reduced to Au^{1+} ions by the ligand shell, and pairs of Au^{3+} and Au^{1+} ions exchange with pairs of Pb^{2+} ions from the perovskite nanocrystal. A primary finding of our earlier study is that Au ions exchange with Pb ions in the nanocrystal whenever the concentration of Au^{3+} is at minimum ~ 2 times greater than the concentration of Pb ions. This cation exchange is an obstacle that needs to be overcome if more refined morphological control over the nanocrystal heterostructure is desired.

Here, we report that the oxidation state of the Au ion determines whether cation exchange or gold deposition occurs when an Au salt is added to solutions of all-inorganic cesium lead halide perovskite nanocrystals. If $CsPbX_3$ nanocrystals are treated with Au(I) halide salts, the surfactant shell of the perovskite reduces Au(I) ions to Au(0) metal that is deposited as nanoparticles on the surface of the nanocrystal. Under these conditions there is no evidence of cation exchange, as indicated by XRD diffraction patterns and PL emission spectra. Alternatively, for $CsPbBr_3$ and $CsPbCl_3$ nanocrystals, the addition of Au(III) halide salts to the perovskite nanocrystal solution promotes conditions that favour complete cation exchange. The exchange products show XRD reflections corresponding to tetragonal $Cs_2Au^{I}Au^{III}Br_6$ or $Cs_2Au^{I}Au^{III}Cl_6$, respectively, and no PL emission across the visible spectrum. Thus, control over the oxidation state of Au is essential for tailoring the morphology and composition of all-inorganic perovskite nanoparticle heterostructures. Using this insight into the role of the gold oxidation state, we report, for the first time, the synthesis of Au-$CsPbCl_3$ and Au-$CsPbI_3$. Remarkably, both display largely unquenched photoluminescence, as has been previously shown for Au-$CsPbBr_3$ nanocrystals.

Experimental details

Materials

Cesium carbonate (Cs_2CO_3, 99.995% trace metals basis), lead (II) bromide ($PbBr_2$, 98%), lead (II) Chloride ($PbCl_2$, 98%), lead (II) iodide (PbI_2, 98%) were purchased from Alfa-Aesar. Oleic acid (OAc, technical grade 90%), oleylamine (OAm, technical grade 70%), Trioctylphosphine (TOP, 97%), 1-octadecene (ODE, technical grade 90%), hexanes (anhydrous mixture of isomers, 99%), toluene (anhydrous, 99.8%), ethanol (EtOH, anhydrous, <0.003% water), gold (III) bromide ($AuBr_3$, 99.9% trace metals basis), gold (III) chloride ($AuCl_3$, 99.9% trace metal basis), gold (I) chloride (AuCl, 99.9% trace metal basis), gold (I) iodide (AuI, 99.9% trace metal basis) were purchased from Sigma Aldrich. Gold (I) monobromide (AuBr, 99.9% trace metals basis) was purchased from City Chemicals LLC.

Synthesis of $CsPbX_3$ Nanocrystals

For this study, cesium lead halide nanocrystals were prepared by modifying a previously published hot-injection method.[26] Briefly, Cs_2CO_3 (0.200 g), OA (0.624 mL), and ODE (10 mL) were added to a 25-mL 3-neck round bottomed flask and heated for 1 hour at 120°C under vacuum to dry. After 1 hour, the flask was put under argon and heated to 150°C until all the Cs_2CO_3 had reacted to form Cs-oleate. The lead halide precursor solution was prepared by dissolving 10 mL of ODE and 0.376 mmol of PbX_2 such as PbI_2 (0.174 g), $PbBr_2$ (0.138 g), or $PbCl_2$ (0.104 g) in a 25 mL 3-neck round bottomed flask and heated under vacuum to 120°C for 1 hour. The solution was then placed under pure argon, and dried OAm (1.0 mL) and dried OA (1.0 mL) were injected to solubilize the PbX_2 salts (1.0 mL of TOP was required to solubilize the $PbCl_2$ salts). The temperature was then increased to 180°C, and the Cs-oleate (0.8 mL) was swiftly injected.

After 5 seconds, the solution was cooled with an ice bath and the final crude solution was centrifuged at 3000 g-forces for 10 minutes, and the supernatant was discarded. The precipitate was then cleaned four times using a combination of ODE and hexane. The final solution was diluted to a final concentration of 0.30 μM. The perovskite nanocrystals concentration was calculated using the molar extinction coefficient, as reported by Maes et al.[30]

Cation exchange reaction

Colloidal $CsPbX_3$ NCs were reacted inside an argon-purged glovebox at room temperature with Au(III) halide salts. Briefly, a stock solution of $AuCl_3$ or $AuBr_3$ was made by solubilizing 80 mg $AuCl_3$ or 113 mg $AuBr_3$ in 0.1 mL of ethanol, and then diluted with 1.0 mL of toluene. For cation exchange reaction, the desired amount of the $AuCl_3$ or $AuBr_3$ stock solution was diluted to a volume of 0.3 mL with toluene to a specific concentration. Next, 0.30 mL of a 0.30 μM $CsPbBr_3$ or $CsPbCl_3$ solution was added to an amber vial and 0.30 mL of the $AuBr_3$ or $AuCl_3$ solution was then swiftly injected. The solutions were stirred for 10 minutes and centrifuged at 3000 g-forces for 10 minutes. The precipitates were suspended in 0.20 mL of anhydrous hexane for further analysis.

Gold metal deposition reaction

All metal deposition reactions were performed inside an argon-purged glovebox at room temperature. First, a stock solution of AuCl, AuBr, or AuI was made by solubilizing 60 mg AuCl, 70 mg AuBr or 83 mg AuI in 0.1 mL of ethanol, and then diluted with 1.0 mL of toluene.

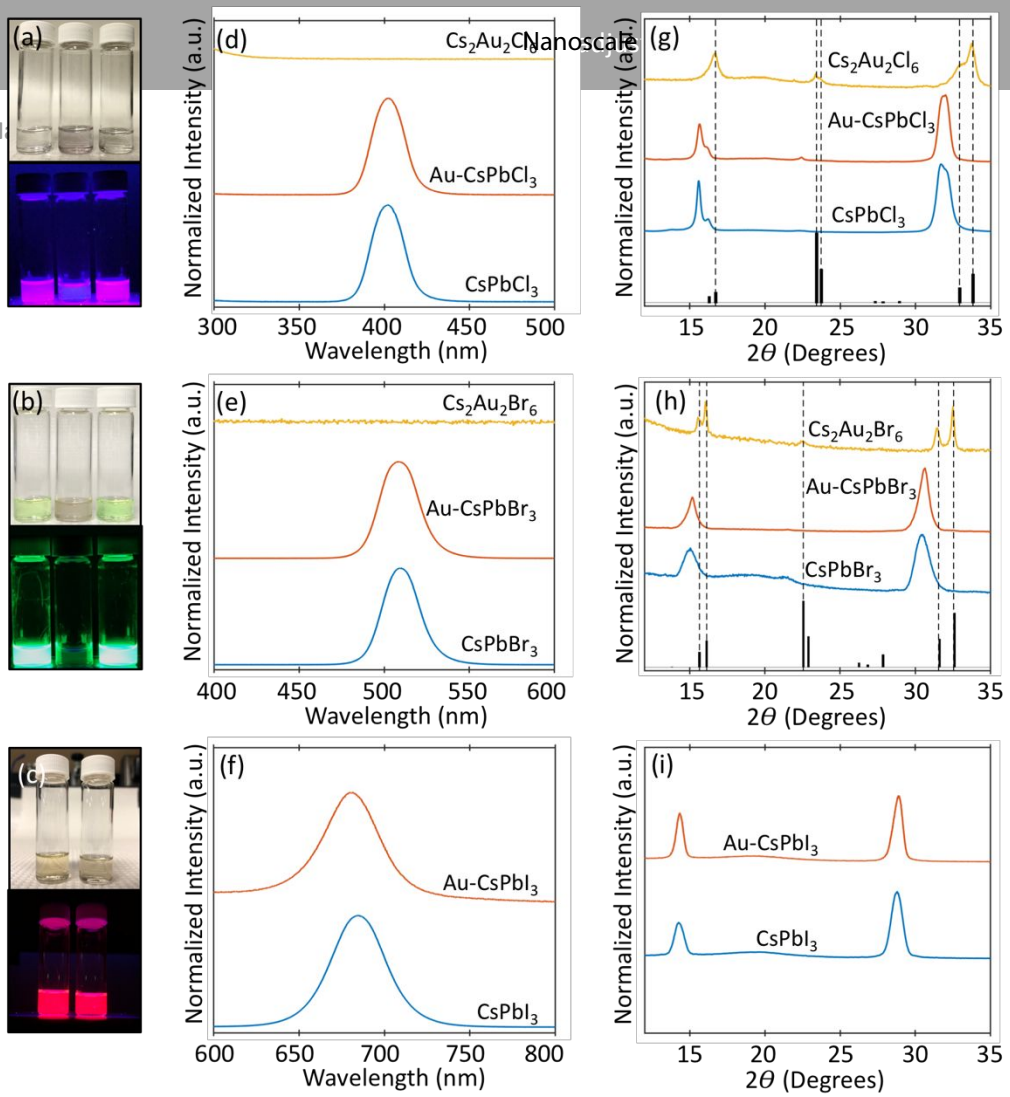

Figure 1. Optical and structural characterization of cesium lead halide nanocrystals before and after gold deposition and cation exchange reactions. (a-c) Photographs of (a) $CsPbCl_3$ (left), $Cs_2Au(I)Au(III)Cl_6$ (middle), and Au-$CsPbCl_3$ (right), (b) $CsPbBr_3$ (left), $Cs_2Au(I)Au(III)Br_6$ (middle) and Au-$CsPbBr_3$ (right), and (c) $CsPbI_3$ (left) and Au-$CsPbI_3$ (right) under white light (top) and 365 nm UV excitation (bottom). (d-f) Photoluminescence emission acquired for (d) $CsPbBr_3$ (blue trace), Au-$CsPbBr_3$ (orange trace), and $Cs_2Au(I)Au(III)Br_6$ (yellow trace), (d) $CsPbCl_3$ (blue trace), Au-$CsPbCl_3$ (orange trace), and $Cs_2Au(I)Au(III)Cl_6$ (yellow trace), and, (e) $CsPbI_3$ (blue trace), and Au-$CsPbI_3$ (orange trace). (g-i) Powder XRD pattern acquired for (g) $CsPbBr_3$ (blue trace), Au-$CsPbBr_3$ (orange trace), and $Cs_2Au(I)Au(III)Br_6$ (yellow trace), (h) $CsPbCl_3$ (blue trace), Au-$CsPbCl_3$ (orange trace), and $Cs_2Au(I)Au(III)Cl_6$ (yellow trace) and, (i) $CsPbI_3$ (blue trace), and Au-$CsPbI_3$ (orange trace). The black ticks on the bottom horizontal axes in (g) and (h) denote reflections of tetragonal $Cs_2Au(I)Au(III)Cl_6$ and tetragonal $Cs_2Au(I)Au(III)Br_6$, respectively.

For Au deposition reactions, the desired amount of the AuCl, AuBr or AuI stock solution was diluted to a volume of 0.3 mL with toluene to a specific concentration. Next, 0.30 mL of a 0.30 μM $CsPbBr_3$, $CsPbCl_3$, or $CsPbI_3$ nanocrystals solution was added to an amber vial and 0.30 mL of the AuBr, AuCl, or AuI solution was then swiftly injected. The solutions were then stirred for 10 minutes followed by centrifugation at 2000 g-forces for 10 minutes. The precipitates were suspended in 0.20 mL of anhydrous hexane for further analysis.

Characterization

High-resolution TEM (HR-TEM) images were obtained using a FEI Tecnai G2 F20 ST instrument operated at an accelerating voltage of 200 kV. Powder X-ray diffraction (XRD) measurements were performed using a Bruker-AXS D8 Advanced Bragg-Brentano diffractometer with a Cu Kα radiation source (λ = 1.5418 Å). Powder XRD data were acquired in the range of 10−35°. PL emission spectra were collected on an Ocean Optics Flame-S-UV-Vis spectrometer with an Ocean Optics DH-200-Bal deuterium and halogen lamp light source. PLQY measurements were measured on a PTI QuantaMaster spectrofluorometer with a xenon arc lamp for steady state excitation. The emission was detected using A PMT (Hamamatsu R928). PLQYs were estimated according to standard procedure using appropriate dye molecules for blue, green and red spectral regions (1,6-Diphenyl-1,3,5-hexatriene, fluorescein, and

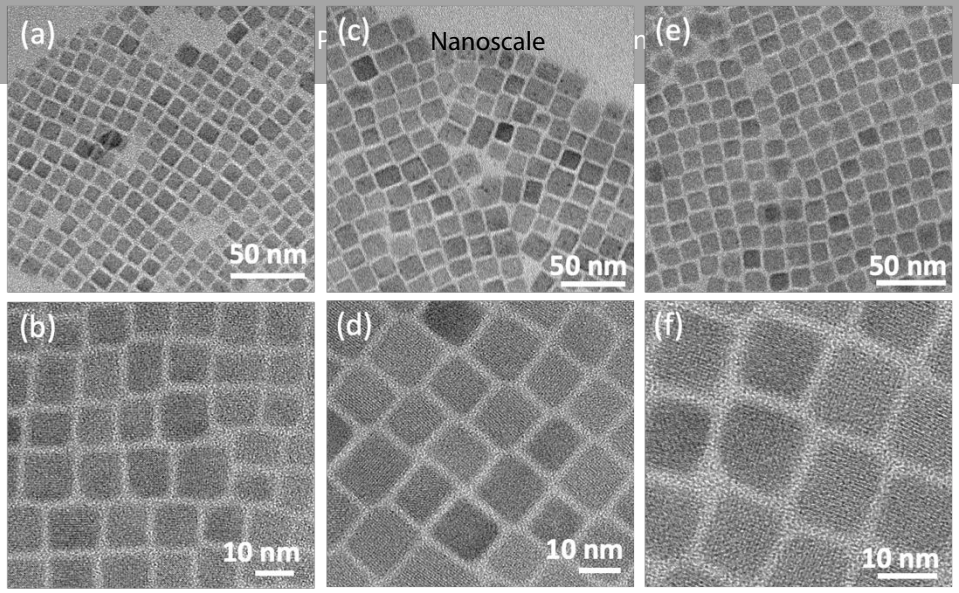

Figure 2. TEM images of as-synthesised $CsPbX_3$ nanocrystals. The top and bottom images show low- and high-magnification TEM images for (a-b) $CsPbCl_3$ nanocrystals, (c-d) $CsPbBr_3$ nanocrystals, and (e- f) $CsPbI_3$ nanocrystals.

rhodamine 6G). All samples were diluted such that their absorbances at the excitation wavelength were comparable.

Result and discussion

Figure 1 highlights differences in the major structural and optical features of $CsPbX_3$ nanocrystals after mixing with Au(I) halide salts or after mixing with Au(III) halide salts. As is clearly observed, the different gold oxidation states are associated with distinct structural and optical characteristics that can be understood to correspond to either Au deposition when Au(I) halide salts are used, or Au cation exchange when Au(III) halide salts are used. We note that Au(III) iodide cannot be readily prepared or purchased,[31] so it was not possible to directly study if Au(III) halide salts could produce $Cs_2Au^{I}Au^{III}I_6$ nanocrystals via a comparable cation exchange reaction.

Figures 1a-c display photographs of colloidal dispersion of as synthesized $CsPbX_3$ nanocrystals (left), after reaction with 0.3 mL of a 6.28 mM Au(III) halide solution (middle), or after reaction with 0.3 mL of a 1.58 mM Au(I) halide solution (right) under ambient light (top) and 365 nm UV excitation (bottom). Interestingly, the colour of the perovskite solution changed immediately upon addition of Au(III) halides from colourless to brown in the case of $CsPbCl_3$ nanocrystals or from green to black for $CsPbBr_3$ nanocrystals (see Figures S1 and S2). In addition, PL emission and clear band edge absorption is lost after $CsPbX_3$ nanocrystals react with AuX_3 solutions as shown in Figure 1 a-b (middle photographs), Figure 1 d-e (yellow traces) and Figures S3-S4 (yellow traces). In contrast, $CsPbX_3$ PL emission and clear band edge absorption is maintained after reaction with Au(I) halide salts, as demonstrated in the rightmost vials in Figure 1 a-c, Figure 1 d-e (orange trace), and Figures S3-S4 (orange traces). PL emission bands characteristic of $CsPbCl_3$, $CsPbBr_3$, and $CsPbI_3$ are observed at 402 nm (Figure 1d, blue trace), at 509 nm (Figure 1e, blue trace), and at 685 nm (Figure 1f, blue trace), respectively.

To better understand the cause of the differences in optical properties before and after reaction with AuX or AuX_3 solution, we performed structural characterization of the products using power X-Ray diffraction as shown in Figure 1g-i. Figure 1g highlights the structural differences in the XRD pattern for $CsPbCl_3$ (blue trace), and the product after reaction of 0.3 mL of a 0.3 mM $CsPbCl_3$ solution with 0.3 mL of a 1.58 mM AuCl solution (orange trace), or 0.3 mL of a 6.28 mM $AuCl_3$ solution (yellow trace). As seen by the XRD pattern, $CsPbCl_3$ nanocrystals and the product of the reaction between $CsPbCl_3$ and AuCl show identical XRD reflections at 2θ values of 15.37, 15.50, and 31.03 degrees that can be attributed to the (100), (020), and (200) crystal planes of orthorhombic $CsPbCl_3$ as reported by Trots and Myagkota.[32] The absence of additional peaks in the XRD diffractogram suggests that Au^{1+} ions do not incorporate into the lattice when the salt is added to solution. In contrast, when $CsPbCl_3$ nanocrystals react with $AuCl_3$, an XRD pattern corresponding to $Cs_2Au^{I}Au^{III}Cl_6$ becomes evident. These XRD peaks can be assigned to (110), (112), (200), (004), (220) reflections of tetragonal phase $Cs_2Au^{I}Au^{III}Cl_6$ as previously determined by Matsushita et al. [33] In this cation exchange reaction, some Au^{3+} ions exchange with Pb without being reduced by the surfactant shell; while some Au^{3+} ions are reduced to Au^{1+} before exchanging with Pb in the perovskite lattice.

The same dependence on the oxidation state of Au was observed for reactions with $CsPbBr_3$ nanocrystals.[29] Figure 1h displays the structural differences for $CsPbBr_3$ (blue trace), and the product after reaction of 0.3 mL of a 0.3 mM $CsPbBr_3$ solution with 0.3 mL of a 1.58 mM AuBr solution (orange trace), or 0.3 mL of a 6.28 mM $AuBr_3$ solution (yellow trace). The diffractogram of $CsPbBr_3$ nanocrystals closely matches the orthorhombic crystal structure reported by Cottingham et al.[34] Similarly, the reaction of $CsPbBr_3$ with AuBr shows only diffraction peaks corresponding to the (002) and (220) planes of orthorhombic $CsPbBr_3$ perovskite, suggesting no exchange of Pb ions by Au ions when AuBr salt is added to the solution of $CsPbBr_3$ nanocrystals. In contrast, when the solution containing $AuBr_3$ is added to the $CsPbBr_3$ solution, reflections of (110), (112), (200), (004), (220) planes can be observed corresponding to the tetragonal crystal phase of $Cs_2Au^{I}Au^{III}Br_6$ as we previously reported.[29, 35] Moreover, consistent

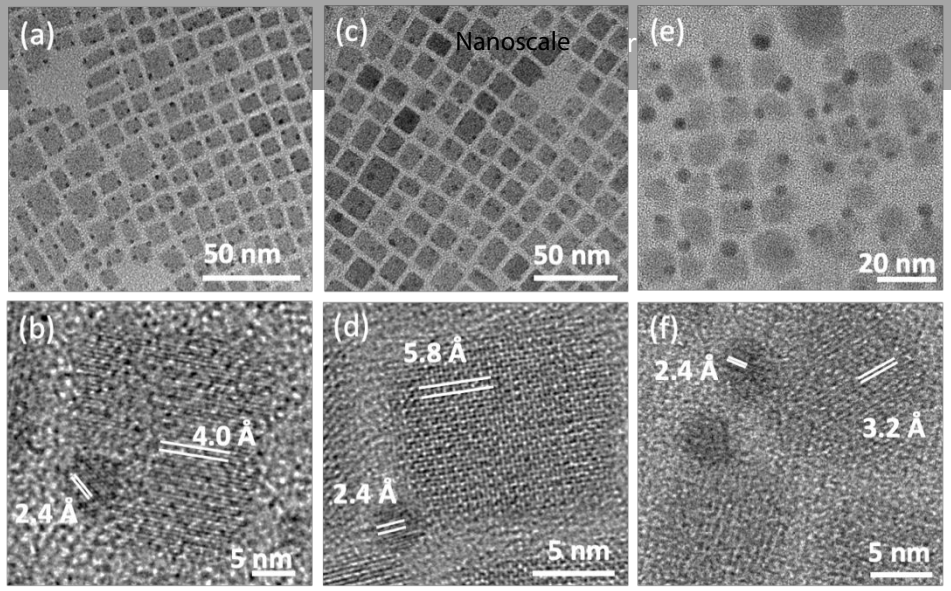

Figure 3. TEM images of $CsPbX_3$ after gold deposition reactions. The top and bottom images show low- and high-magnification TEM images for (a-b) Au-$CsPbCl_3$ heterostructures, (c-d) Au-$CsPbBr_3$ heterostructures, and (e- f) Au-$CsPbI_3$ heterostructures. (b) Lattice-resolved HRTEM images acquired for an (b) Au-$CsPbCl_3$ heterostructure indicating lattice spacing corresponding to the (110) plane of orthorhombic $CsPbCl_3$ (4.0 Å) and the (111) plane of cubic Au (2.4 Å), (d) for an Au-$CsPbCl_3$ heterostructure indicating lattice spacing corresponding to the (202) plane of orthorhombic $CsPbBr_3$ (5.8 Å) and the (111) plane of cubic Au (2.4 Å), and (f) for an Au-$CsPbI_3$ heterostructure indicating lattice spacing corresponding to the (212) plane of orthorhombic $CsPbI_3$ (3.2 Å) and the (100) plane of cubic Au (2.4 Å).

with this general trend, XRD patterns acquired for $CsPbI_3$ and the reaction between 0.3 mL of a 0.3 mM $CsPbI_3$ solution and 0.3 mL of a 1.58 mM AuI solution are nearly identical. The peaks observed at 2θ values of 14.10, and 28.81 degrees closely matches recent results by Sutton and coworkers indicating the orthorhombic phase of $CsPbI_3$ (Figure 1i).[36]

To further determine the presence of Au nanoparticles on the surface of $CsPbX_3$ nanocrystals and to obtain insights into the morphology changes associated with Au deposition and cation exchange, we performed high-resolution transmission electron microscopy (HR-TEM) of the obtained product after reaction of $CsPbX_3$ nanocrystals with AuX or AuX_3 salt. Figure 2 shows low- (top) and high- (bottom) magnification TEM images acquired for as-synthesized $CsPbCl_3$ (figure 2a-b), $CsPbBr_3$ (figure 2c-d), and $CsPbI_3$ nanocrystals (figure 2e-f) with uniform cuboidal morphology and average lateral dimensions of 8-10 nm (see Figures S6-S8 for more TEM images). Figure 3 shows low- (top) and high- (bottom) magnification electron micrographs for the same batch of $CsPbX_3$ nanocrystals after reaction with 0.30 mL of the corresponding 1.58 mM AuX salt solutions. Au nanoparticles can be clearly observed on the corners and edges of $CsPbX_3$ nanocrystals as dark points of contrasts. It has been previously proposed that nucleation of Au ions on the corner and edges of the perovskite may be influenced by the lower ligand density coverage at these positions.[28] Additionally, these points of contrast have lattice spacings that can be resolved by HR-TEM corresponding unequivocally to the lattice separation between (111) planes of cubic gold (Figures 3b,3d, and 3f and Figures S9-S11). Lattice spacing between planes corresponding to the orthorhombic phase of $CsPbX_3$ perovskite nanocrystals can also be resolved, confirming no exchange of Au^{1+} ions with Pb ions in the perovskite lattice (Figures 3b,3d, and 3f). For instance, separations between (110) plane in $CsPbCl_3$, (202) plane in $CsPbBr_3$, and (212) plane in $CsPbI_3$ can be resolved with lattice spacing of 4.0 Å, 5.8 Å, and 3.2 Å, respectively.

Surprisingly, $CsPbX_3$ retains comparable PLQY when Au metal nanoparticles are deposited onto the surface of the perovskite (Table S1). In particular, Au-$CsPbBr_3$ and Au-$CsPbI_3$ heterostructures retain remarkable PLQY of 52.07 % and 23.05 %, respectively, that are far more luminescent in comparison with similar hybrid Au−chalcogenide nanoparticle heterostructures (for which complete quenching of band edge photoluminescence has been observed).[22] Maintaining such relatively high PLQYs while in contact with Au nanoparticles suggests that Au−$CsPbX_3$ heterostructures may offer new opportunities for optoelectronic device applications such as luminescence up-conversion. In fact, a recent study by our group have shown that $CsPbBr_3$ nanocrystals coupled to plasmonically active gold nanoparticles can enhance anti-Stokes photoluminescence (ASPL).[37]

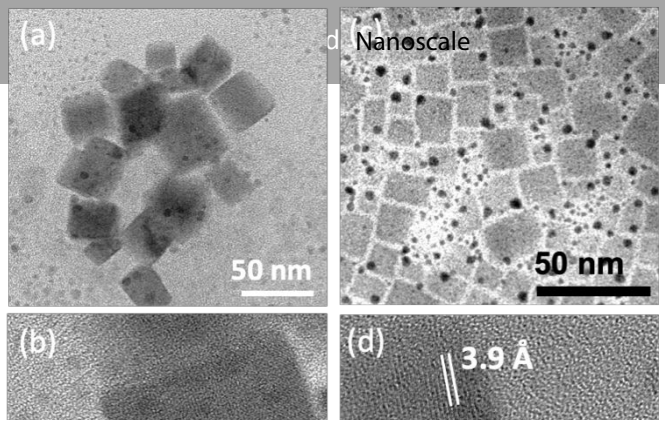

Figure 4. TEM images of $CsPbX_3$ after cation exchange reactions. The top and bottom images show low- and high-magnification TEM images for (a-b) $Cs_2Au(I)Au(III)Cl_6$ nanocrystals, and (c-d) $Cs_2Au(I)Au(III)Br_6$ nanocrystals. (b) HRTEM image of $Cs_2Au(I)Au(III)Cl_6$ NCs showing lattice spacing of 3.8 Å corresponding to the separation between the (112) planes of tetragonal $Cs_2Au(I)Au(III)Cl_6$. (d) HRTEM image of $Cs_2Au(I)Au(III)Br_6$ NCs showing lattice spacing of 3.9 Å corresponding to the separation between the (122) planes of tetragonal $Cs_2Au(I)Au(III)Br_6$.

In comparison, visible PL was completely quenched for the $CsPbX_3$ perovskite nanocrystals treated with AuX_3 solutions as shown in Figures 1d and 1e. As previously discussed, this is a direct result of the cation exchange. Figure 4 shows low- (top) and high- (bottom) magnification electron micrographs acquired for nanocrystals when 0.3 mL of a 6.28 mM $AuCl_3$ solution and 6.28 mM $AuBr_3$ solution are added to solutions of $CsPbCl_3$ (left) and $CsPbBr_3$ (right) nanocrystals, respectively. As shown in Figure 4, both structures show similar cuboidal morphology as their parent $CsPbCl_3$ or $CsPbBr_3$ nanocrystals. However, the perovskite particle size appears to increase after undergoing cation exchange, from an edge length of 8-9 nm before the reaction to an edge length spanning 22-45 nm after complete cation exchange. Several possibilities may account for this size change, including an instability of the parent $CsPbX_3$ nanoparticles to cation exchange, or destabilization of the ligand shell during sample cleaning. However, we cannot exclude a more complex mechanism leading to particle aggregation as the size of the exchange nanocrystals are significantly larger than the parent $CsPbX_3$ perovskites. Nevertheless, these structures have resolved lattice spacings of 3.8 Å and 3.9 Å corresponding to the d-spacing of (112) and (122) planes of tetragonal $Cs_2Au^IAu^{III}Cl_6$ and $Cs_2Au^IAu^{III}Br_6$, respectively, further confirming complete cation exchange of Pb ions in the perovskite lattice (Figure 4Bb and 4d).

It is worth mentioning that the above Au deposition and cation exchange procedures were performed at two different concentrations, namely, 1.58 mM AuX for Au deposition and 6.28 mM AuX_3 for cation exchange. The concentration of 6.28 mM AuX_3 was used for cation exchange as pure $Cs_2Au^IAu^{III}X_6$ could be obtained. Clear evidence of cation exchange, however, still occurs when a 1.58 mM solution of AuX_3 is used, as indicated by XRD (Figure S12 and S14). However, when a 6.28 mM solution of AuX is used only diffraction peaks corresponding to orthorhombic phase $CsPbX_3$ are evident (Figure S13 and S15). In addition, Au deposition still occurs when 6.28 mM solution of AuX reacts with $CsPbX_3$ nanocrystals (as demonstrated in Figure S16 and S17). These comparisons highlight that the final product is solely dependent on the oxidation state of the Au ions across these concentration regimes.

Conclusions

We have demonstrated the role of the gold oxidation state in the reaction of gold halide salts with all-inorganic lead halide perovskite nanocrystals. When AuX is added to a solution of $CsPbX_3$ nanocrystals, gold deposition occurs. However, when an equivalent amount of AuX_3 is added to $CsPbX_3$, cation exchange occurs. Optical and structural measurements indicate that Au-$CsPbX_3$ heterostructure nanoparticles preserve comparable PLQY and identical crystal structure as the parent $CsPbX_3$ nanocrystals. In contrast, the cation exchange products, $Cs_2Au^IAu^{III}Br_6$ or $Cs_2Au^IAu^{III}Cl_6$ show no PL emission in the visible spectrum. Our results elucidate the important role of the oxidation state of Au salts for determining the outcome of reactions to produce all-inorganic perovskite nanoparticle heterostructures.

Conflicts of interest

The authors declare no competing financial interest.

Acknowledgements

This work is funded in part by the Gordon and Betty Moore Foundation through Grant GBMF6882 and by the Air Force Office of Scientific Research under award number FA9550-16-1-0154. M.S. also acknowledges support from the Welch Foundation (A-1886).

Notes and references

1. N. Waiskopf, Y. Ben-Shahar and U. Banin, *Adv Mater*, 2018, **30**, e1706697.
2. H. Wang, L. Zhang, Z. Chen, J. Hu, S. Li, Z. Wang, J. Liu and X. Wang, *Chem Soc Rev*, 2014, **43**, 5234-5244.
3. L. Zhang and M. Jaroniec, *Applied Surface Science*, 2018, **430**, 2-17.
4. M. T. Sheldon, P. E. Trudeau, T. Mokari, L. W. Wang and A. P. Alivisatos, *Nano Lett*, 2009, **9**, 3676-3682.
5. D. V. Talapin, J. S. Lee, M. V. Kovalenko and E. V. Shevchenko, *Chem Rev*, 2010, **110**, 389-458.
6. H. Wang, F. Liu, W. Fu, Z. Fang, W. Zhou and Z. Liu, *Nanoscale*, 2014, **6**, 12250-12272.
7. U. Banin, Y. Ben-Shahar and K. Vinokurov, *Chemistry of Materials*, 2014, **26**, 97-110.

8. R. Costi, A. E. Saunders and U. Banin, *Angew Chem Int Ed Engl*, 2010, **49**, 4878-4897.
9. M. J. Enright and B. M. Cossairt, *Chem Commun (Camb)*, 2018, **54**, 7109-7122.
10. S. K. Dutta, S. K. Mehetor and N. Pradhan, *J Phys Chem Lett*, 2015, **6**, 936-944.
11. E. Shaviv, O. Schubert, M. Alves-Santos, G. Goldoni, R. Di Felice, F. Vallee, N. Del Fatti, U. Banin and C. Sonnichsen, *ACS Nano*, 2011, **5**, 4712-4719.
12. W. Shi, H. Zeng, Y. Sahoo, T. Y. Ohulchanskyy, Y. Ding, Z. L. Wang, M. Swihart and P. N. Prasad, *Nano Letters*, 2006, **6**, 875-881.
13. G. Dukovic, M. G. Merkle, J. H. Nelson, S. M. Hughes and A. P. Alivisatos, 2008, **20**, 4306-4311.
14. J. Maynadie, A. Salant, A. Falqui, M. Respaud, E. Shaviv, U. Banin, K. Soulantica and B. Chaudret, *Angew Chem Int Ed Engl*, 2009, **48**, 1814-1817.
15. T. Mokari, C. G. Sztrum, A. Salant, E. Rabani and U. Banin, *Nature Materials*, 2005, **4**, 855.
16. Y. Shemesh, J. E. Macdonald, G. Menagen and U. Banin, *Angew Chem Int Ed Engl*, 2011, **50**, 1185-1189.
17. G. Menagen, J. E. Macdonald, Y. Shemesh, I. Popov and U. Banin, *J Am Chem Soc*, 2009, **131**, 17406-17411.
18. G. Menagen, D. Mocatta, A. Salant, I. Popov, D. Dorfs and U. Banin, *Chemistry of Materials*, 2008, **20**, 6900-6902.
19. T. Mokari, E. Rothenberg, I. Popov, R. Costi and U. Banin, *Science*, 2004, **304**, 1787-1790.
20. A. E. Saunders, I. Popov and U. Banin, *J Phys Chem B*, 2006, **110**, 25421-25429.
21. L. Amirav and A. P. Alivisatos, *The Journal of Physical Chemistry Letters*, 2010, **1**, 1051-1054.
22. A. Demortiere, R. D. Schaller, T. Li, S. Chattopadhyay, G. Krylova, T. Shibata, P. C. dos Santos Claro, C. E. Rowland, J. T. Miller, R. Cook, B. Lee and E. V. Shevchenko, *J Am Chem Soc*, 2014, **136**, 2342-2350.
23. T. Shanmugapriya and P. Ramamurthy, *The Journal of Physical Chemistry C*, 2013, **117**, 12272-12278.
24. Q. A. Akkerman, G. Raino, M. V. Kovalenko and L. Manna, *Nat Mater*, 2018, **17**, 394-405.
25. M. V. Kovalenko, L. Protesescu and M. I. Bodnarchuk, *Science*, 2017, **358**, 745-750.
26. L. Protesescu, S. Yakunin, M. I. Bodnarchuk, F. Krieg, R. Caputo, C. H. Hendon, R. X. Yang, A. Walsh and M. V. Kovalenko, *Nano Lett*, 2015, **15**, 3692-3696.
27. A. Swarnkar, R. Chulliyil, V. K. Ravi, M. Irfanullah, A. Chowdhury and A. Nag, *Angew Chem Int Ed Engl*, 2015, **54**, 15424-15428.
28. S. K. Balakrishnan and P. V. Kamat, *ACS Energy Letters*, 2017, **2**, 88-93.
29. B. J. Roman, J. Otto, C. Galik, R. Downing and M. Sheldon, *Nano Lett*, 2017, **17**, 5561-5566.
30. J. Maes, L. Balcaen, E. Drijvers, Q. Zhao, J. De Roo, A. Vantomme, F. Vanhaecke, P. Geiregat and Z. Hens, *J Phys Chem Lett*, 2018, **9**, 3093-3097.
31. T. Sohnel, R. Brown, L. Kloo and P. Schwerdtfeger, *Chemistry*, 2001, **7**, 3167-3173.
32. D. M. Trots and S. V. Myagkota, *Journal of Physics and Chemistry of Solids*, 2008, **69**, 2520-2526.
33. N. Matsushita, H. Ahsbahs, S. S. Hafner and N. Kojima, *Review of High Pressure Science and Technology*, 1998, **7**, 329-331.
34. P. Cottingham and R. L. Brutchey, *Chem Commun (Camb)*, 2016, **52**, 5246-5249.
35. N. Matsushita, ukuhara, Fumiya, and Kojima, Norimichi, *Acta Crystallographica Section E*, 2005, **1600-5368**.
36. R. J. Sutton, M. R. Filip, A. A. Haghighirad, N. Sakai, B. Wenger, F. Giustino and H. J. Snaith, *ACS Energy Letters*, 2018, **3**, 1787-1794.
37. B. J. Roman and M. Sheldon, *Nanophotonics*, 2019, **8**, 4, 599–605.

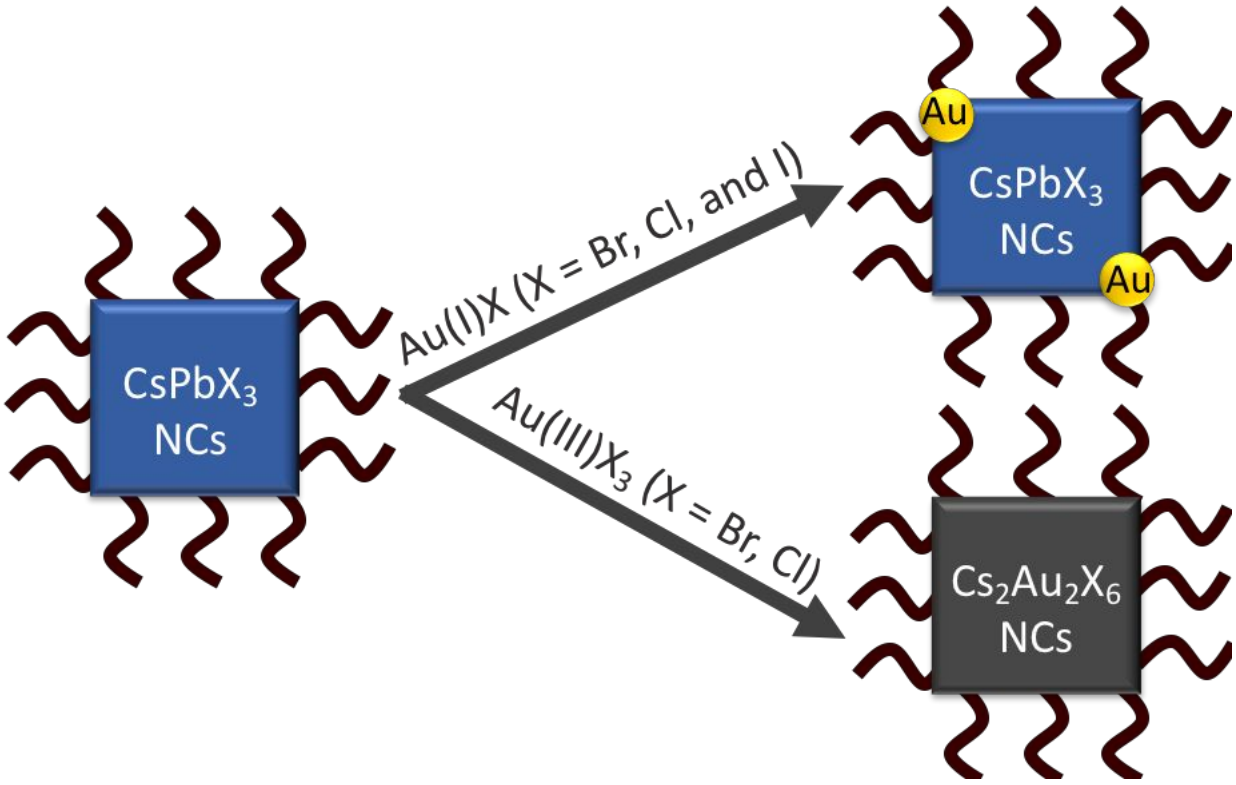

Graphical Abstract. The oxidation state of the Au ions determines whether cation exchange or gold deposition occurs when an Au salt is added to solutions of all-inorganic cesium lead halide perovskite nanocrystals.